Department of Physics and Astronomy
University of Heidelberg

Bachelor Thesis in Physics
submitted by

Timo Gierlich

born in Kirchheim unter Teck (Germany)

2017

Design of a fiber-coupled argon laser spectroscopy and investigation of the metastable density in an RF source

This Bachelor Thesis has been carried out by Timo Gierlich at the
Kirchhoff-Institute for Physics in Heidelberg
under the supervision of
Prof. Dr. Markus K. Oberthaler

Abstract:

The atom-trap trace analysis experiment relies on multiphoton scattering in a magneto-optical trap to detect the rare ^{39}Ar below the 10^{-15} level. The argon atoms are excited to the metastable $1s_5$ (J = 2) state in a plasma in order to make them accessible for laser cooling. To lock the laser frequency to the used cooling transition from $1s_5$ (J = 2) to $2p_9$ (J = 3), a saturated absorption spectroscopy is needed as a reference. For this purpose, a fiber-coupled closed spectroscopy cell was developed in the scope of this work. The core of this spectroscopy cell is a closed argon glass cell in which a plasma is ignited via RF discharge in a helical resonator.

Additionally, the three-dimensional density distribution of metastable argon in the source chamber was investigated via laser spectroscopy. By measuring the optical depth perpendicular to the flow direction of the atoms, the radial distribution could be determined by an Abel inversion. The preliminary results support a non-Gaussian distribution whose maximum is located in a ring around the symmetry axis.

Zusammenfassung:

Das ATTA-Experiment beruht auf Mehrphotonenstreuung in einer magneto-optischen Falle zur Detektion des seltenen ^{39}Ar -Isotop unterhalb der 10^{-15}-Schwelle. Um die Argonatome der Laserkülhung zugänglich zu machen, werden sie in einem Plasma in den metastabilen $1s_5$ (J = 2) Zustand angeregt. Eine dopplerfreie Sättigungsspektroskopie wird wird als Referenz verwendet, um die Laserfrequenz auf den Kühlübergang von $1s_5$ (J = 2) zu $2p_9$ (J = 3) einzustellen. Für diesen Zweck wurde eine fasergekoppelte geschlossene Spektroskopiezelle im Rahmen dieser Arbeit entwickelt. Das Herzstück ist dabei eine geschlossene Argongaszelle, in der ein Plasma mittels RF-Entladung in einem Helix-Resonator gezündet wird.

Darüber hinaus wurde die dreidimensionale Dichteverteilung metastabiler Argonatome in der Quellkammer mittels Laserspektroskopie untersucht. Es wurde die optische Tiefe orthogonal zur Flussrichtung der Atome gemessen, woraus die radiale Verteilung mit Hilfe einer inversen Abeltransformation berechnet wurde. Die Ergebnisse sprechen für eine nicht-gaußförmige Verteilung, deren Maximum ringförmig um die Symmetrieachse angesiedelt ist.

Contents

1. Introduction

The dating of water and ice samples is of great interest in environmental sciences. The age of water gives important information about transport and mixing processes in the groundwater, continental water and oceans as well as in the cryosphere. The determination of the age of such a sample is based on the measurement of radioactive tracers that are dissolved in the water. In this context, the age of water refers to the point in time when the water sample had its last contact with the atmosphere and the gas exchange ceased leaving the radioisotopes to decay.

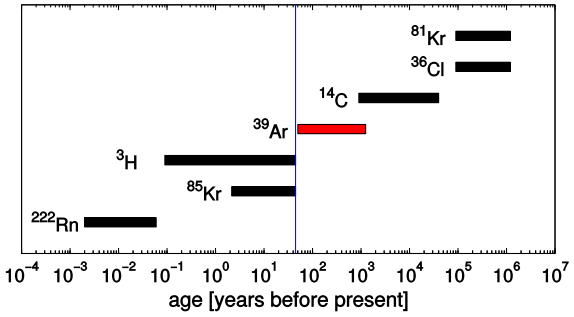

Figure 1.1.: Dating ranges for radioactive isotopes commonly used in water dating. ^{39}Ar has half-life of 269 years and therefore closes the dating gap between 50 years and 1000 years.

Each radioactive tracer has its own dating range depending on its half-life which is depicted in fig. 1.1. ^{39}Ar has a half-life of 269 years that leads to a dating range of 50 years to 1000 years. ^{39}Ar would be a perfect environmental tracer, for instance it is as a noble gas chemically inert, if its abundance wasn't that low, namely 8.23×10^{-16}, which makes routine analysis difficult[1] [1]. For this purpose Atom Trap Trace Analysis (ATTA) was developed at first for krypton and adapted to argon (ArTTA).

ATTA exploits the shift of the optical resonance frequency due to differences in mass and nuclear spin between the abundant and the rare isotopes to detect the rare ones like ^{39}Ar . Although one single resonant excitation is not sufficient to distinguish between

[1]This correspond to 8500 ^{39}Ar atoms in a liter of water, or to illustrate it a bit, this is comparable to a black corn of rice in a convoy of trucks reaching around the equator, each loaded with 40 t of rice [1].

the radioisotope and the huge background of abundant isotopes, many cycles of photon absorption and spontaneous emission in a magneto-optical trap (MOT) ensure a sufficient selectivity and sensitivity [2]. The schematic of the current experimental setup is depicted in fig. A.1 on page 32.

Currently, a new experimental setup – the ArTTA-10ml beamline – is under construction which will be available for routine measurements. During this Bachelor thesis a new fiber-coupled closed spectroscopy cell was developed for this setup which is used for locking the reference laser to the cooling transition (see section 2.1 on the following page) that is used for the laser cooling of the atoms. The other lasers are tuned to this frequency. In this context, a helical resonator for the RF discharge of a argon plasma cell was built and characterized. Furthermore, a manufacturing process for the plasma cells was developed.

The extremely low abundance of ^{39}Ar combined with a relatively inefficient plasma source limits the count rate of the apparatus which requires long measuring times in order to achieve sufficiently low statistical errors. At the moment, the ArTTA apparatus runs at a count rate of 6 atoms per hour with a source efficiency in the order of 1×10^{-4}. Therefore improvements of the source are promising for increasing the count rate and consequently the statistical errors. During this work, three dimensional measurements of the density distribution of metastable argon atoms were carried out. This can help for a better understanding of the processes in the source chamber and developments towards a more efficient plasma source design.

2. Theory

2.1. Optical properties of argon

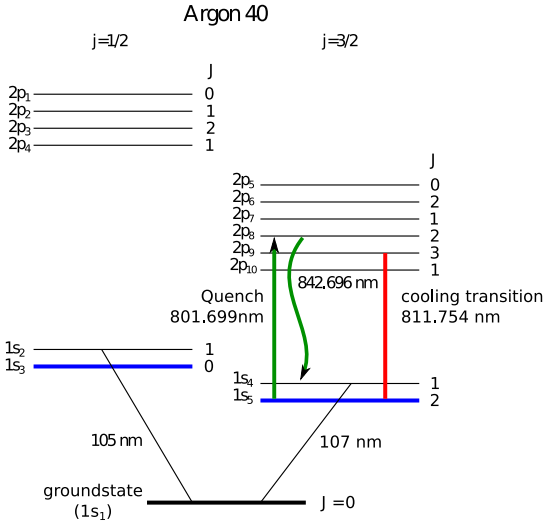

Figure 2.1.: Energy spectrum of ^{40}Ar . The states are given in the Paschen notation. As the two possible transitions from the groundstate to the $1s_2$ (J = 1) and $1s_4$ (J = 1) lie in the deep UV spectrum, argon atoms must be excited to a metastable state (here $1s_5$) in order to use them for laser cooling. For that the cycling transition from $1s_5$ (J = 2) to $1p_9$ (J = 3) is used. Additionally, the transition from $1s_5$ (J = 2) to $1p_8$ (J = 2) can be used for removing the atoms from the cooling cycle. ^{39}Ar has also a hyperfine structure that is relevant for ATTA, but wasn't of importance in the measurements of this work (adapted from [1]).

The nature of argon's energy spectrum can be understood by having a look at the electron configuration the argon atom. It is a noble gas because it has a closed valence shell. This leads to a very stable electron configuration and consequently very high energy levels and a high ionization energy. In this work all states are given in the Paschen notation. ATTA is based on laser cooling and trapping of atoms. However, transitions from the ground state to either $1s_2$ (J = 1) or $1s_4$ (J = 1) lie with a wavelength of approximately 105 nm and 107 nm respectively in the deep UV range [2] (see fig. 2.1). As UV light in this range is absorbed by air and neither conventional lasers nor optics

are available for these wavelengths, the argon atoms are excited to the metastable $1s_5$ (J = 2) state which is done with an argon plasma which is described in section 2.3 on page 8. A disexcitation back to the ground state is forbidden because of $\Delta J = 2$ and the lifetime of this state is $\approx 38\,\mathrm{s}$.

The cycling transition from $1s_5$ (J = 2) to $2p_9$ (J = 3) with $\lambda = 811.754\,\mathrm{nm}$ is perfectly suitable for the cooling transition. Besides, the transition from $1s_5$ to $2p_8$ ($\lambda = 802\,\mathrm{nm}$) is used as a depumping transition to remove atoms from the cooling cycle.

In contrast to the stable argon isotopes that have even numbers of nucleons[1] ^{39}Ar has a nuclear spin $I = 7/2$ that leads to a hyperfine splitting of the fine structure levels with the quantum number J into $|2J + 1|$ sublevels. The nuclear spin $\vec{I}$ couples with the total electronic angular momentum $\vec{J}$ to the new total momentum $\vec{F} = \vec{J} + \vec{I}$ with $|J - I| \leq F \leq |J + I|$.

2.2. Laser spectroscopy

This paragraph recaps the basics of laser spectroscopy that are necessary for the subsequent chapters; a good overview can be found in [3]. Here, we deal with a two-level system like the cooling transition.

2.2.1. Atom-light interaction

Consider an ideal two-level system with the resonance frequency ω_0. When this system is exposed to laser light with the frequency ω_l, the atom absorbs and emits photons with the excitation rate

$$\gamma_s = \frac{\gamma}{2} \frac{s}{1 + s + 4\delta^2/\gamma^2} \tag{2.1}$$

where $\gamma = \frac{1}{\tau}$ is the spontaneous decay rate which is the inverse of the transition's life-time, $\delta = \omega_0 - \omega_l$ denotes the detuning of the laser and $s = I/I_s$ the saturation parameter that describes the ratio of the laser intensity I to the saturation intensity I_s of the transition [4].

In case of the used cooling transition the life-time $\tau = 27.09\,\mathrm{ns}$ and consequently $\gamma = 2\pi \cdot 5.87\,\mathrm{MHz}$. as well as $I_s = 28.8\,\mathrm{W\,m^{-2}}$[1] for linear polarized light.

The line shape profile for resonant absorption is given by a Lorentzian (fig. 2.2a on the next page)

[1] ^{36}Ar, ^{38}Ar and ^{40}Ar are stable. ^{40}Ar has a natural abundance of about 0.996.

$$\mathcal{L}(\omega_0, \omega_l) = \frac{1}{1 + 4\delta^2/\gamma^2}. \tag{2.2}$$

Here, γ corresponds to the width of the distribution. It originates from the state's finite life-time τ and the uncertainty principle;

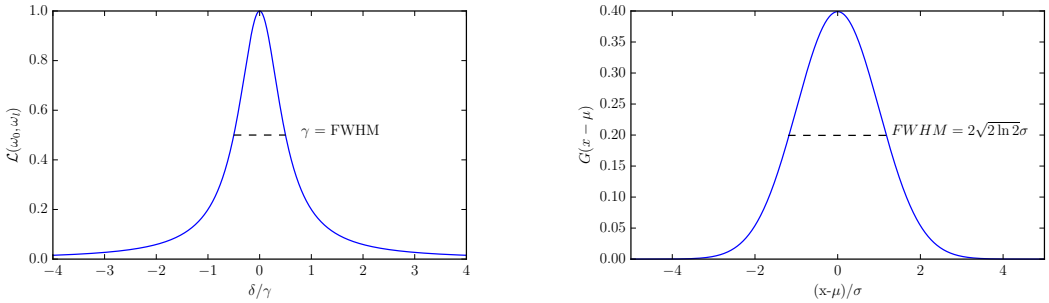

(a) Lorentzian distribution **(b)** Gaussian distribution

Figure 2.2.: Comparison of the two absorption profiles. The Lorentzian distribution eq. (2.2) comes from the finite life-time τ of the state. It's full width half maximum (FWHM) is equal to the spontaneous decay rate $\gamma = 1/\tau$. The Gaussian distribution in the absorption profile has its origin in the random walk of the argon atoms. The FWHM is given by $2\sqrt{2\ln 2} \cdot \sigma$.

2.2.2. Laser absorption spectroscopy

A simple experimental setup for a laser absorption spectroscopy is shown in fig. 2.3. A laser beam propagates through a vapor cell and the transmitted intensity is measured by a photo diode. The laser frequency is scanned through a small interval around the natural resonance frequency ω_0 of a certain transition. As the laser beam passes through the gas, the atoms absorb photons and are excited to the higher energy level. Subsequently photons are emitted again in all spatial direction by spontaneous emission. This will cause an attenuation of the incident beam which is recorded by the photo diode.

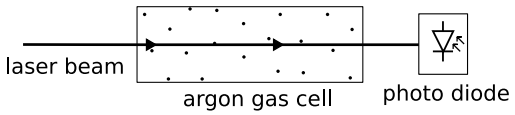

Figure 2.3.: Schematic of a simple laser spectroscopy. A laser beam propagates through a vapor cell and is attenuated by the gas atoms depending of the detuning δ. The frequency of the laser can be tuned. A photodiode measures the transmitted intensity.

When having a closer look at the real absorption profile we will observe that its shape

is not Lorentzian and much broader than expected – typically too broad to distinguish hyperfine structure lines in the spectrum. This effect is called Doppler broadening. In order to understand this, the random thermal motion of the gas atoms must be considered [5]. The probability $P_v(v)\mathrm{d}v$ to find an atom with a velocity component v parallel to the laser beam – the perpendicular component is invisible for the laser – in the interval $[v, v + \mathrm{d}v]$ is given by

$$P_v(v)\mathrm{d}v = \sqrt{\frac{m}{2\pi k_B T}} \exp\left(-\frac{mv^2}{2k_B T}\right) \mathrm{d}v, \tag{2.3}$$

where $k_B = 1.38 \times 10^{-23}\,\mathrm{J\,K^{-1}}$ denotes the Boltzmann constant, m the atomic mass (here $m_{Ar} = 39.95\,\mathrm{u}$) and T the temperature of the gas in Kelvin. This corresponds to a Gaussian distribution

$$P_v(v)\mathrm{d}v = \frac{1}{\sqrt{2\pi}\sigma_v} \exp\left(-\frac{v^2}{2\sigma^2}\right) \mathrm{d}v \tag{2.4}$$

with $\mu = 0$ (the mean velocity vanishes) and a standard deviation

$$\sigma_v = \sqrt{\frac{k_B T}{m}}. \tag{2.5}$$

These thermal motions lead to a Doppler shift

$$\omega_D = \omega_0 \left(1 + \frac{v}{c}\right), \tag{2.6}$$

where c is the speed of light.

Now we want to express the distribution in terms of the frequency $f = \frac{\omega}{2\pi}$

$$P_f(f)\mathrm{d}f = P_v(v)\frac{\mathrm{d}v}{\mathrm{d}f}\mathrm{d}f. \tag{2.7}$$

If we use eq. (2.6) the distribution will read

$$P_f(f)\mathrm{d}f = \sqrt{\frac{mc^2}{2\pi k_B T f_0^2}} \exp\left(-\frac{mc^2(f - f_0)^2}{2k_B T f_0^2}\right) \mathrm{d}f. \tag{2.8}$$

One can immediately see that the standard deviation is given by

$$\sigma_f = \sqrt{\frac{k_B T}{mc^2}} f_0. \tag{2.9}$$

Please note that at room temperature ($T \approx 293\,\mathrm{K}$) it is $\sigma_f \approx 300\,\mathrm{MHz}$ for the cooling transition, whereas its hyperfine structure is in the same order of magnitude.

2.2.3. Saturated absorption spectroscopy

Since the hyperfine splitting of energy levels cannot be distinguished by using a simple technique as described above, more advanced methods are required. The saturated absorption spectroscopy helps to avoid this problem (see fig. 2.4).

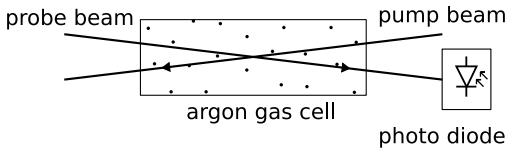

Figure 2.4.: Setup of a saturated absorption spectroscopy. In addition to the setup described in section 2.2.2 on page 5 a second laser beam from the same laser is installed. This so called pump beam points in the opposite direction as the probe beam and depletes the ground state population. Ideally, both beams should have a large area where they overlap.

Here, a second laser beam that is counter propagating to the first one, now called probe beam, is installed. It comes from the same laser but, has a comparably high intensity which is about ten times higher than the other one and is called pump beam. It depletes the population in the ground state until the ground and excited state equilibrate; in the maximum case the two populations are equal. The transition is then said to be saturated, which is the origin of the techniques name. However, this happens only very close to the resonance frequency. To understand the effect on the probe beam, we have to look at two different cases.

Firstly, we examine atoms with $v = 0$. As stated above, half of the ground state population is pumped to the upper level so that the probe beam "sees" less atoms in the ground state. This "burns" a hole in the absorption profile of the probe beam. It has the shape of a Lorentzian with the natural line width γ plus effects like pressure and power broadening [3] and is called *Lamb dip*.

Secondly, the atoms with $v \neq 0$ see both the pump beam and the probe beam Doppler shifted. The Doppler shift for the pump beam has another sign than the one for the probe beam because they propagate in the opposite direction. This leads to the fact that the pump beam burns a hole in a velocity group that is far away from the velocity group that is in resonance with the probe beam. Consequently, these atoms only contribute to the normal Gaussian profile.

As a result, one obtains a Doppler broadened absorption profile that has a Lamp dip at the resonance frequency (see fig. 3.7 on page 19).

2.3. Introduction to plasma physics

The avid reader finds an elaborate introduction to plasma physics in [6]. Here, a short recap of plasma physics is presented that is useful for understanding the next chapters.

A plasma – often called the fourth state of matter – is a collection of free charged particles that is, on average, electrically neutral. The particles in a plasma move in random direction. In this work only weakly ionized plasma is of importance[2]. It is characterized by the following features: Firstly, the plasma is driven electrically. Secondly, collisions between charged particles and neutral atoms are of importance. Thirdly, surface losses at boundaries are important. Fourthly, the ionization of neutral atoms sustains the plasma in the steady state and last but not least, the electrons are not in thermal equilibrium with the surroundings and the gas particles.

In our applications we only use low-pressure discharge in an order of $> 1 \times 10^{-6}$ mbar[3]. Here, the light and heavy charged particles are never in thermal equilibrium, i.e. $T_e \gg T_i$, where T_e describes the electron and T_i the ion temperature. As the discharge is electrically driven, the applied power heats mostly the electrons because their mass is about a factor of some thousands smaller than that of the positive ions.

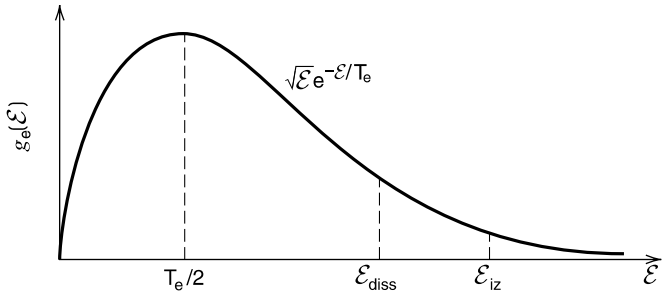

Figure 2.5.: Energy distribution $g_e(\mathcal{E})$ of the electrons in a weakly ionized plasma discharge. The function is not necessarily a Maxwell-Boltzmann distribution. Note, that only the high-energy part contributes to the ionization and dissociation processes (taken from [6]).

Normally, T_e is less than the threshold energies for ionization or dissociation $\mathcal{E}_{iz}$ and $\mathcal{E}_{diss}$, which means that only the high-energy tail of the energy distribution, that is shown in fig. 2.5, contributes to the ionization and dissociation.

For ArTTA, metastable argon atoms are required rather than ionized atoms. It proves that a RF (radio frequency) discharge leads to a sufficient flux of metastable atoms [2].

[2] Highly ionized plasma is mainly found in the universe where stars and much of interstellar matter is plasma.

[3] In the experiments he pressure was measured close to the walls, it is higher in the region where the plasma burns.

For the ArTTA apparatus an antenna coil is used (see section 4.1.1 on page 21) whereas the fiber-coupled closed spectroscopy cell makes use of a helical resonator that is described in section 3.3 on page 13 in detail.

3. Fiber-coupled closed spectroscopy cell

3.1. Design of the spectroscopy module

The stability of the lasers is a key requirement for the measuring process with ArTTA since a drift in the wavelength during the measuring procedure would cause systematical errors. This mainly results in a lower count rate and hence reduce the accuracy of the dating result. Therefore the lasers for the ArTTA apparatus must be precisely locked to a certain wavelength. As a reference for the laser system the cooling transition from $1s_5$ to $2p_9$ with $\lambda = 811.754\,\text{nm}$ of ^{40}Ar is used.

For this purpose a modular fiber-coupled closed spectroscopy cell was designed during this work. Its functional principle is based on a saturated absorption spectroscopy which is described in the previous chapter.

The main design criteria were stability as well as modularity and flexibility. Stability refers to a long operation time without any maintenance. The cell should be insensitive to any disturbance like vibrations, temperature changes etc. The plasma cell itself has only a limited lifetime of approximately half a year (cf. section 3.2 on page 12) so this cell can also be quickly replaced. Modularity and flexibility mean that this device runs independent from the remaining laser system, is compact and can be installed separately from the optical table which is a great advantage since the space for optical installations is rather limited in the ArTTA-10ml container. Since it is fiber-coupled, it can be easily replaced or connected to another laser.

Figure 3.1 on the next page shows the schematic of the spectroscopy cell. The design was executed with the CAD software *SolidWorks*. The construction consists of an aluminum block of 380 mm x 140 mm x 50 mm where the optical and electrical components plus helical resonator are mounted. The incoming light through a fiber is coupled out and collimated with a lens tube construction which can be rotated. Now follows a periscope made of two silver mirrors that gives the necessary four degrees of freedom for the alignment of the laser beam. The beam passes a polarizing beam splitter cube (PBS) which can be used for adjusting the beam's intensity: The polarization angle of the beam is attuned by rotating the lens tube which determines how much light can pass straight

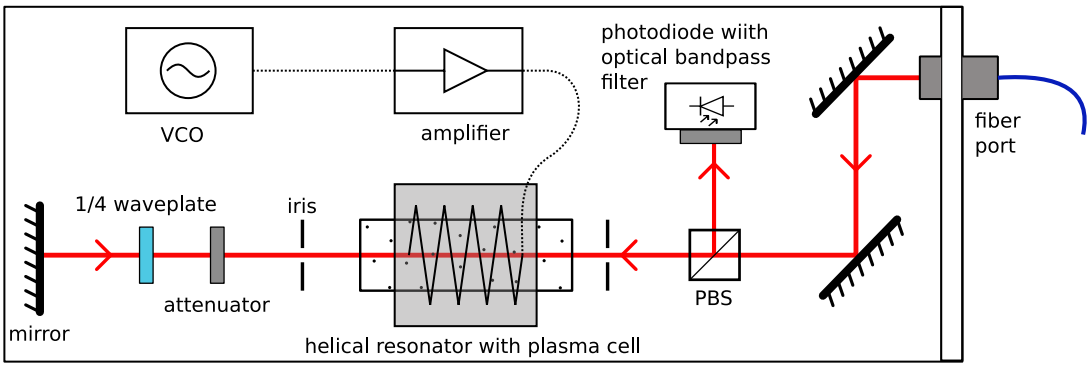

Figure 3.1.: Schematic of the fiber-coupled closed spectroscopy cell. A voltage controlled oscillator (VCO) generates a high-frequency signal ($\approx 60\,\mathrm{MHz}$), which is amplified by a 1 W-amplifier and is fed in the helical resonator.

through the PBS and how much is refracted. The straight path is now s-polarized. Both irises on each side of the plasma cells are required for the exact alignment of the beam. The plasma itself is generated with a helical resonator (see sections 2.3 and 3.3 on page 8 and on page 13). Here, the high-frequency signal is generated by a voltage controlled oscillator (VCO) and then amplified with a 1 W RF-amplifier.

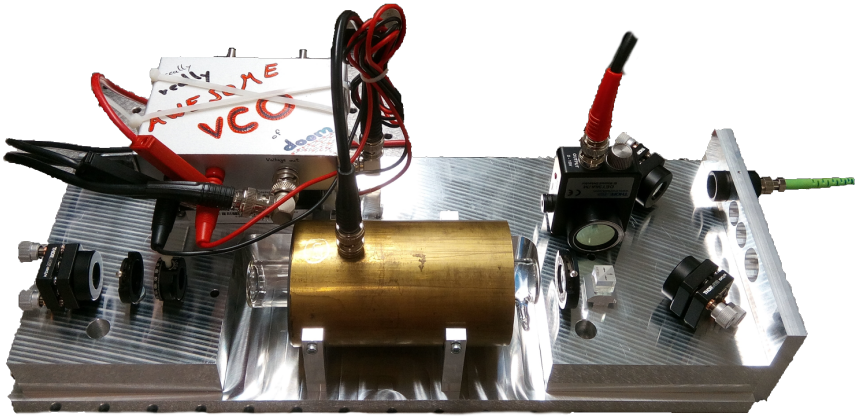

Figure 3.2.: Photography of the assembled spectroscopy cell.

Then the beam goes through a $\lambda/4$ - waveplate and an attenuator and is finally reflected at a mirror back to the PBS. The $\lambda/4$ - waveplate must be aligned such that the beam is now p-polarized and all of the light is refracted to the photodiode[1].

[1]It should be avoided that light enters the fiber again because this can form a cavity in the previous

The parts of the spectroscopy cell, namely the ground plate, the front plate and the holders for the helical resonator, were manufactured in the institute's workshop.

3.2. Manufacturing of closed argon plasma cells

We manufactured the plasma cells for the fiber-coupled closed spectroscopy cells with the help of the glassblowery in the 'Zentralbereich Neuenheimer Feld'. The apparatus for that is shown in fig. 3.3. The plasma cell is 6 inch long, 1 inch in diameter and is made of DURAN glass. For filling it is mounted on a long glass tube with a valve in the middle (V1) and a KF flange on the other side. This is connected with a T-piece to a pump station and a argon gas bottle via a dosing valve (V2). The pump station consists of a turbomolecular pump and a forepump and a produces a high vacuum in the order of 1×10^{-6} mbar in the cell.

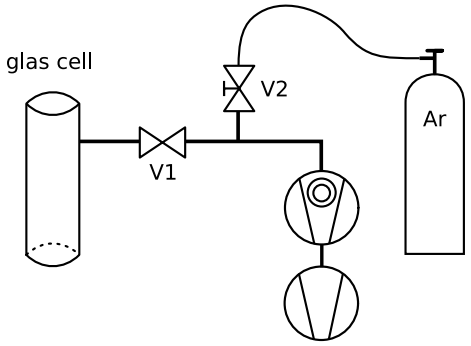

Figure 3.3.: Schematic of the filling apparatus. The glass cell consists of a round tube where a long glass tube with a valve (V1) is mounted. It is connected to a pump station that produces a high vacuum. The gas flow from the argon gas bottle can be regulated the dosing valve (V2).

The filling process starts with the evacuation of the glass cell. V1 is open and V2 is closed. When the pressure has reached its minimum, V2 is opened carefully and argon can inflow into the system. Unfortunately, there was no gauge available for monitoring the pressure. Instead, the rotational speed of the turbomulecular pump was used as an indicator. As soon as the speed fell below a critical value, we assumed that enough argon gas is in the cell. V1 and then V2 is closed again and a plasma is ignited in the cell by a helical resonator. This cleans the cell because the plasma sputters impurities out of the glass walls. During this process the plasma changed its color from pink to white which indicates that the whole procedure can be started again. The process is repeated

parts of the laser system which causes fringes in the signal.

several times until the plasma's color doesn't change anymore. We experienced that a pink plasma burn longer than a white one. Now, V1 is closed and the cell can be melt off by the glassblowery in the 'Zentralbereich Neuenheimer Feld'. Typically, one cell lasts for half a year, then it must be replaced.

As an improvements of the manufacturing process the installation of a gauge is planned which would ensure a reproducible gas inflow. Moreover, a spectroscopy of the plasma would provide information about the involved substances. This could help understand why the color of the plasma changes during the cleaning and to determine the moment when the cleaning is finished.

3.3. Construction and characterization of a helical resonator

This section is mainly based on [7].

Normally, helical resonators are used in high frequency technology where they serve as compact narrow bandpass filter for applications in the HF and VHF ranges[2]. Helical resonators have typically high quality factors Q that can exceed 1000. Q is a measure for the damping of an oscillating system. In this case they proved to be optimal for a RF discharge plasma cell.

Reasons why we chose a helical resonator for the closed spectroscopy cell instead of the open antenna design of the source (see section 4.1.1 on page 21) are numerous. One advantage is the shielding of the helical resonator. It reduces the RF power that is radiated into the lab. This could cause disturbance in other electrical devices in the lab when the RF signal couples in. Secondly, the helical resonator can be run with less power that the open antenna. For the resonator a 1 W-amplifier is sufficient whereas the antenna in the source chamber needs a 35 W-amplifier. This makes the electronic equipment simpler and reduced again the RF-power emitted in the lab. Moreover, the helical resonator has a well defined resonance frequency and input impedance, which ensures that the plasma ignites reliably and makes a additional impedance matching unnecessary.

[2] High frequency (HF) refers to the frequency range between 3 and 30 MHz, very high frequency (VHF) to the range between 30 and 300 MHz.

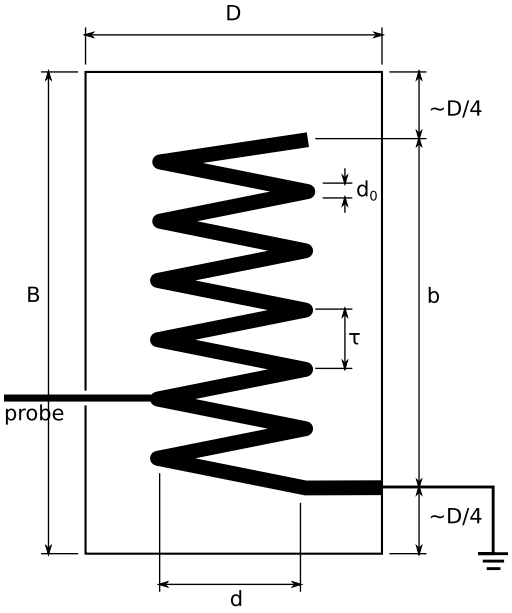

(a) Sketch of a helical resonator. In our design we used the following dimensions and materials: The shielding is made of a brass tube with B = 110 mm, D = 65 mm. The coil is made of a enameled copper wire with a cross-sectional area of 4 mm x 1 mm, τ = 8 mm, a diameter d = 34 mm, a total length b = 90 mm and a total number of turns N = 12.

(b) As a probe connection a BNC-plug was used. At the ends ringlike PVC caps are inserted where the plasma glass cell is fixated. The impedance of the closed end Z_{end} should be matched to the wave impedance of the coaxial cable ($\approx 50\,\Omega$) to reduce reflections of the signal back to the amplifier.

Figure 3.4.: Helical resonator for RF plasma discharge, resonance frequency $\approx$ 60 MHz. It is designed for the fiber-coupled closed spectroscopy cell.

Design criteria and theory The following relations and equations are taken from [7] and transformed in the SI unit system. They are mainly derived empirically.

We designed the helical resonator for an unloaded resonance frequency $f_0 \approx 60\,\mathrm{MHz}$ and a shielding diameter $D = 65\,\mathrm{mm}$. The dimensions of the resonator which are depicted in fig. 3.4a on page 14 are calculated according to these relations (length in mm, frequencies in MHz):

- $N = \frac{48000}{f_0 D}$
- $\frac{d}{D} = 0.55$
- $\frac{b}{d} > 1.0$
- $B \approx b + \frac{d}{2}$
- $\tau < \frac{d}{2}$

From that we chose $B = 110\,\mathrm{mm}$. The coil is made of copper wire with $d_0 = 4\,\mathrm{mm}$, $\tau = 8\,\mathrm{mm}$, a diameter $d = 34\,\mathrm{mm}$, a total length $b = 90\,\mathrm{mm}$ and a total number of turns $N = 12$.

The empirical equation for inductance per axial cm of long solenoid with a shielding reads

$$L = 0.4 \cdot n^2 d^2 \left[1 - \left(\frac{D}{d}\right)^2\right] \mu\mathrm{H\,cm^{-1}} \approx 0.13\,\mu\mathrm{H\,mm^{-1}}. \tag{3.1}$$

The self capacitance per axial cm of the coil and the fringing field at the top of the coil is given by

$$C = \frac{0.3}{\log(D/d)}\,\mathrm{pF\,cm^{-1}} \approx 0.26\,\mathrm{pF\,mm^{-1}}. \tag{3.2}$$

This yields a characteristic impedance

$$Z_0 = \sqrt{LC} \approx 1100\,\Omega. \tag{3.3}$$

The quality factor of the unloaded resonator can be calculated by

$$Q_u = 20 \cdot D\sqrt{f_0} \approx 1000. \tag{3.4}$$

The helical resonators were connected to a vector network analyzer (VNA) for measuring the frequency response in a range from 20 MHz to 200 MHz. The result is depicted

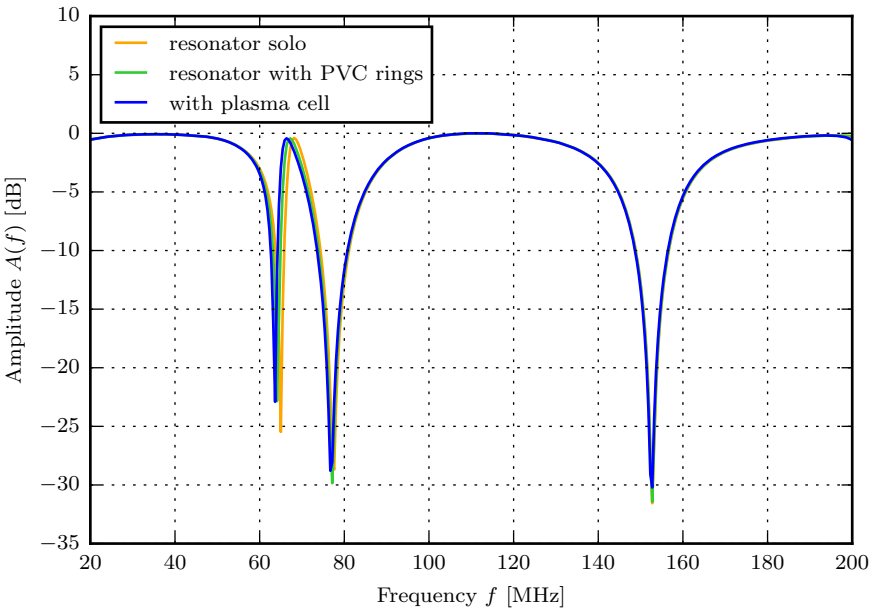

Figure 3.5.: Frequency response of a self made helical resonator recorded by a vector network analyzer (VNA). The first peak belongs to the projected resonace frequency of 60 MHz. One important feature is that the resonance frequency will shift to smaller values if a load like the PVC rings or the plasma tube is inserted. The other peaks come from effects like reflections and the influence of the cable.

in fig. 3.5 on page 16. Three configurations were examined. The blue graph shows the unloaded resonator, the green line shows it with the PVC rings on both ends and the orange line with PVC rings and the plasma tube, but without a plasma burning.

Three peaks are visible at 65 MHz, 78 MHz and 135 MHz. The left one belongs to the resonance frequency of the helical resonator. It is quite close to the projected frequency of 60 MHz. One important feature is that the resonance frequency will shift to smaller values if a load like the PVC rings or the plasma tube is inserted. They increase the capacitance of the resonator, because these materials are dielectric and therefore have relative electrical permittivies $\epsilon_r > 1$. The other three peaks don't exhibit this behavior. This leads to the assumption that they come from other effects like reflections in the cable.

Additionally, the resonators were tested with a burning plasma cell. We weren't able to measure a frequency response with a burning plasma because the RF signal from the antenna that produces the plasma would be coupled in the helical resonator and distort the result. We observed that the optimal frequency for igniting the plasma is dependent on the cell the same as the resonance frequency of the of the helical resonator with plasma cell, and the frequency where the plasma burns best is approximately 2 MHz lower because the plasma also serves a load for the resonator.

3.4. Measurements with the closed spectroscopy cell

The raw data of a saturated absorption spectroscopy realized with the closed spectroscopy cell are presented in fig. 3.6 on the following page. A diode laser "DL Pro" from Toptica Photonics was used as light source. Additionally, a Fabry-Pérot interferometer[3] (FPI) with a free spectral range was used for the frequency calibration of the x-axis together with the position of the lamb dip which defines the zero.

Both a normal spectroscopy and a background signal without plasma are measured since the optical properties of the glass cell are frequency dependent. To remove them, the spectroscopy signal was divided by the background. The result is shown in the blue curve in fig. 3.7 on page 19. A Gaussian curve was fitted to the absorption profile,

$$f(x) = a \exp\left(-\frac{(x-\mu)^2}{2\sigma^2}\right) + b, \tag{3.5}$$

for which the values $a = -0.642 \pm 0.03$, $\mu = (6 \pm 2)\,\text{MHz}$, $\sigma = (375 \pm 2)\,\text{MHz}$ and $b = 0.998 \pm 0.001$ were obtained. The temperature of the gas can be calculated with

[3]Here, the FPI set up in [8] was used.

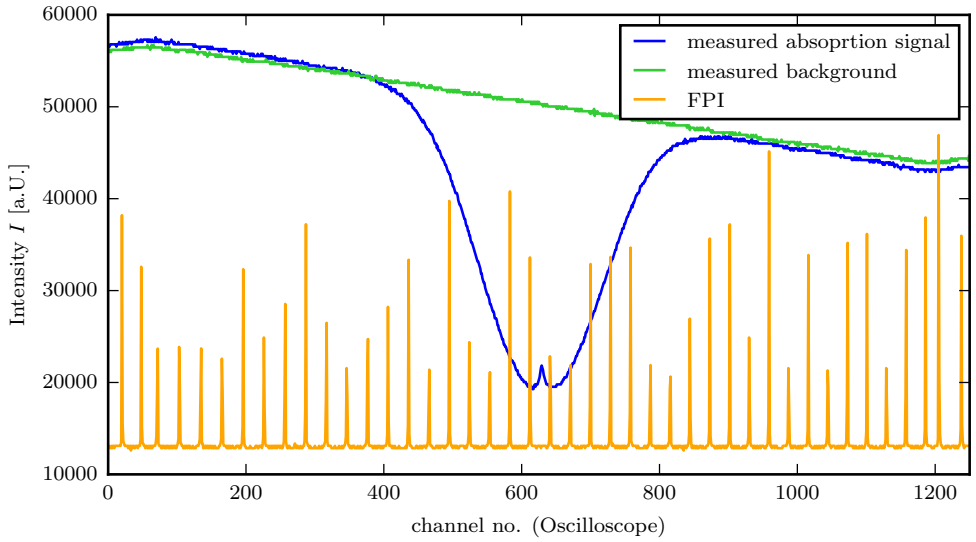

Figure 3.6.: Measured raw data. The signal from the saturated absorption spectroscopy, a background signal and the FPI signal is plotted. The x-axis shows the channel number of the oscilloscope's A/D converter and the y-axis the 16-bit value. Although the background signal exhibit a slope, the lab dip of the saturated absorption spectroscopy is prominent enough to use it for locking the laser.

eq. (2.9) on page 6. We obtain $T = (445 \pm 5)\,\mathrm{K}$. This is higher than room temperature but it appears to be a realistic value. The pressure in the plasma cell is very low ($< 1 \times 10^{-6}\,\mathrm{mbar}$) which is why the thermal conductivity of the plasma is small and the glass cell doesn't feel that hot when touching it.

Figure 3.8 on page 20 shows a closeup of the Lamb dip. The Gaussian curve that was determined in the previous step is subtracted from the measured data points and a Lorentzian

$$f(x) = \frac{a}{1 + 4(x - x_0)^2/\gamma^2} + b \tag{3.6}$$

is fitted afterwards. This yields $a = 0.059 \pm 0.004$, $x_0 = (3 \pm 2)\,\mathrm{MHz}$, $\gamma = (46 \pm 4)\,\mathrm{MHz}$ and $b = 0.014 \pm 0.003$. The theoretical value for the spontaneous decay rate is $\gamma_{theo} = 2\pi \cdot 5.87\,\mathrm{MHz} = 36.9\,\mathrm{MHz}$. Possible deviations from the theory can occur because of effects like power and pressure broadening, that haven't been taken into account.

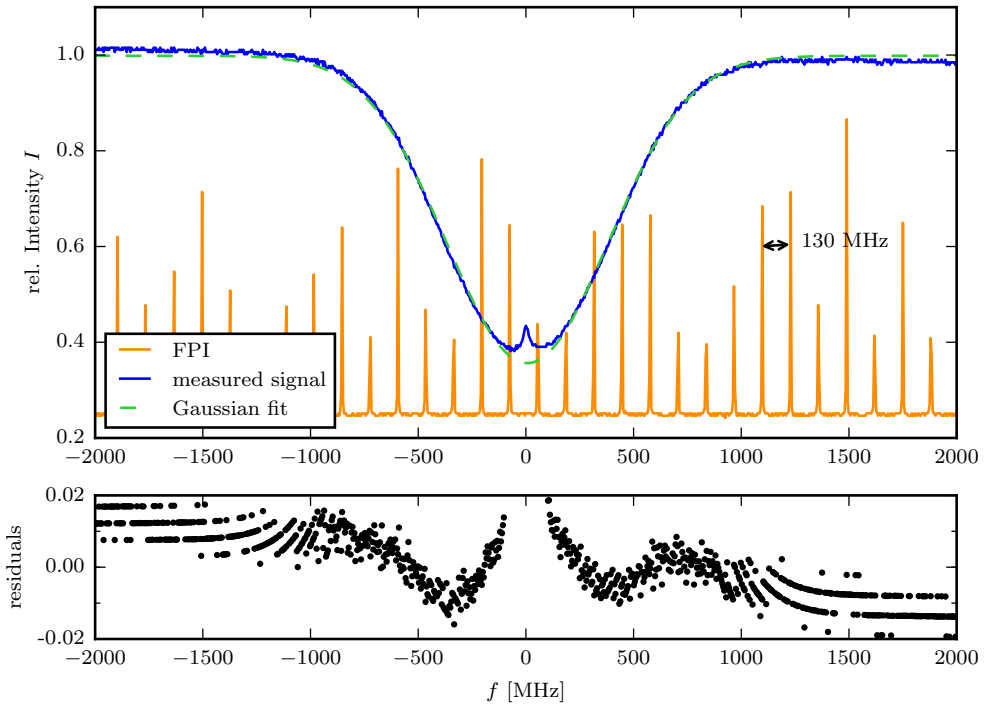

Figure 3.7.: Results of the measurement of the cooling transition with the fiber-coupled closed spectroscopy cell. The blue line shows the measured signal after the background was removed. A Gaussian is fitted to the curve, the residuals are depicted in the lower graph. Additionally, the Fabri-Pérot signal (orange) is plotted.

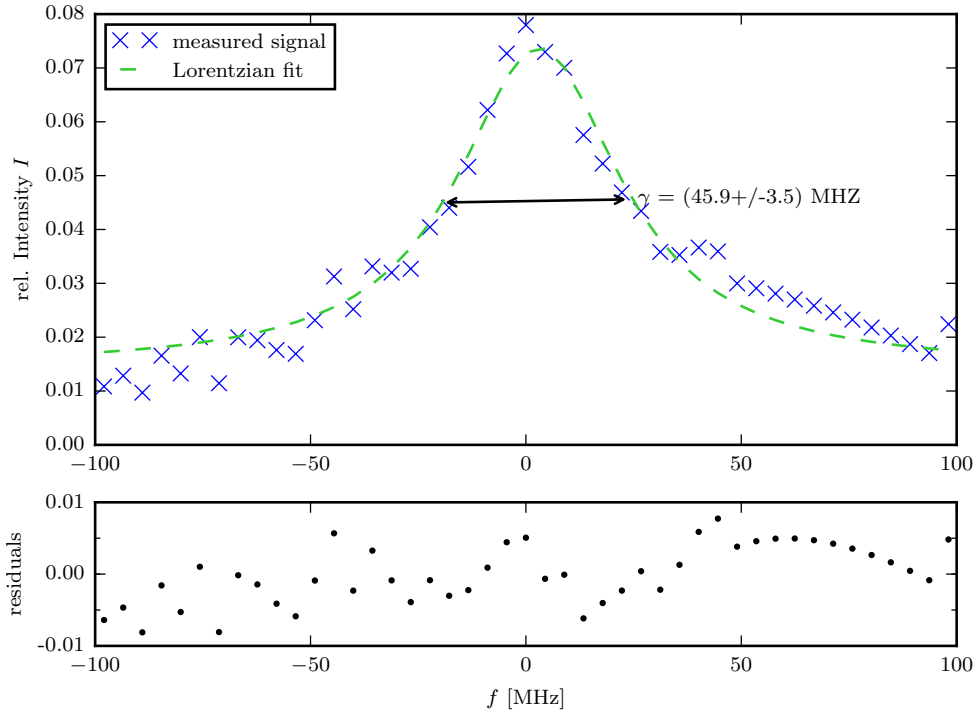

Figure 3.8.: Lamb dip of the saturated absorption spectroscopy. The blue crosses represent the measured data points minus the Gaussian distribution. Here, a Lorentzian is fitted to the data.

4. Characterization of the plasma source

As mentioned in section 2.1 on page 3, argon cannot be excited from the ground state with conventional optics and lasers. Therefore the atoms are excited to the metastable $1s_5$ state by using a plasma source to make them accessible for laser cooling. An improvement of this step is desired since the production rate of these metastable atoms limits the count rate and consequently the performance of the dating process. At the moment the ArTTA-apparatus reaches a counting rate of approximately 6 atoms per hour.

A precise characterization of the plasma source helps to understand the underlying processes of the production of metastable argon which could lead to a redesign of the source chamber. In the following section three-dimensional measurements of the plasma source performed on OpTTA-apparatus and their results are presented.

4.1. Experimental setup

For the optimization of the plasma source a vacuum apparatus called OpTTA (abbreviation for "Optimizing Trap Trace Analysis") was build up [9]. Here we can perform measurements on the plasma, analyze parameters like pressure or temperature of the inflowing gas that might affect the density of metastable argon as well as experimentalize with different source and antenna designs without occupying valuable measuring time at the normal ArTTA beam lines. Appart from that, with OpTTA we can use enriched samples which would contaminate the ArTTA machines.

The OpTTA apparatus consists of two vacuum chambers that are connected via an aperture. Figure 4.1 on the next page shows a schematic of the vacuum system. Oil diffusion pumps provide high pumping speed which is why modifications at the apparatus can be quickly realized. The left chamber contains the plasma source that is designed to be identical to that used in the current ArTTA apparatus.

4.1.1. The plasma source

The source consists of a ceramic tube where the argon gas flows through. Around this tube a coil made of 1 mm x 4 mm isolated copper wire is installed which serves as a RF

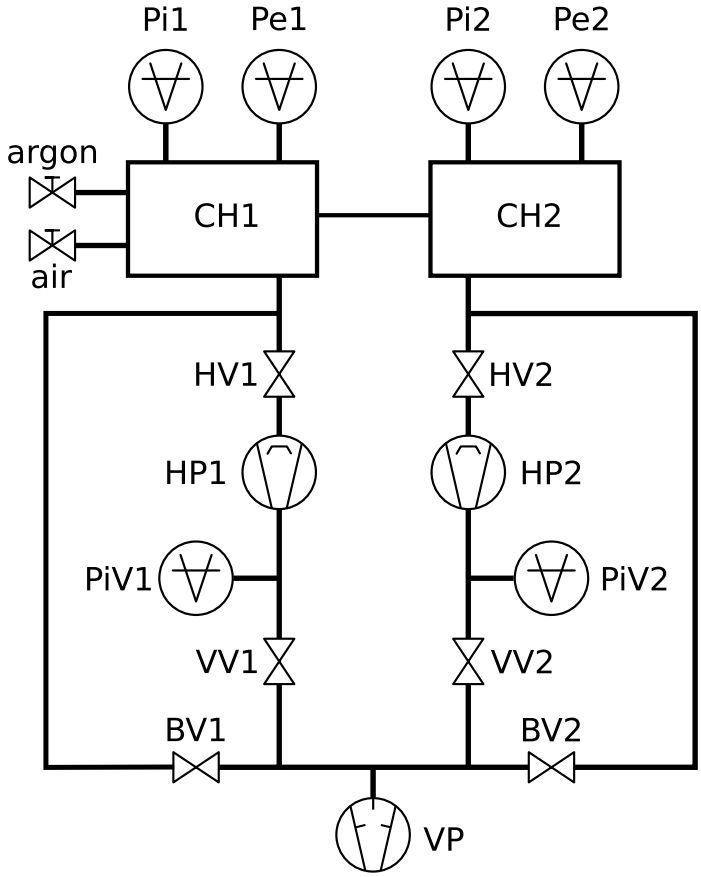

Figure 4.1.: Vacuum system of the OpTTA apparatus. Each vacuum chamber (CH1 and CH2) is pumped to a high vacuum (1×10^{-5} mbar) by an oil diffusion pump (HP1 and HP2), the pressure is monitored by a Pirani gauge (Pi1 ad Pi2) as well as by a Penning gauge (Pe1 and Pe2). The Pirani gauges work in a pressure range form atmospheric pressure to 5×10^{-4} mbar whereas Penning gauges work at pressures below 1×10^{-4} mbar. CH1 has a dosing valve for argon, that is connected to the source, and one for air that is used for venting the chamber. The fore-vacuum is produced by a rotary vane pump (VP) and is monitored by the Pirani gauges PiV1 and PiV2. Valves HV1 and HV2 seal off the high vacuum in the chambers and the bypass valves BV1 and BV2 are opened to evacuate CH1 and CH2 to the fore-vacuum level.

antenna. It has 10 windings at a diameter of 35 mm and a length of 45 mm and a total length of 1.2 m that is matched with the wavelength of the RF signal. Normally, the source is cooled with liquid nitrogen because this increases metastable flux rate after collimator[1] [10] (see fig. A.1 on page 32). Here we omit cooling because it shouldn't affect the outcome of the measurements. The cooling of the inflowing gas reduces the longitudinal and transversal velocity component of the atoms in the same way. This is why the distribution of metastables isn't effected qualitatively.

4.1.2. Measuring procedure

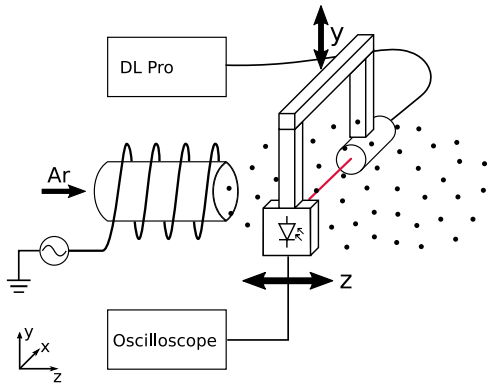

(a) Schematic of the experiment. Laser light from the diode laser DL Pro is coupled into a fiber. The U-shaped frame can be moved in y- and z-direction.

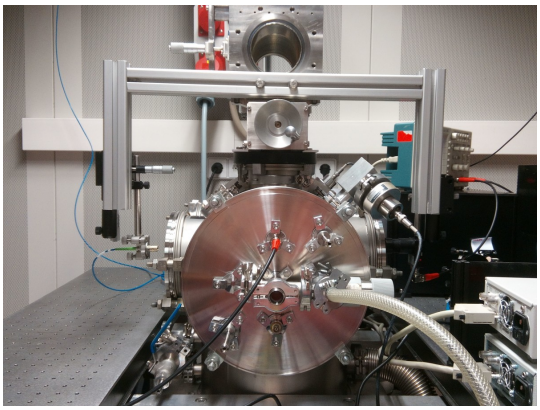

(b) Photo of the construction. In absence of a translation stage with a large traveling path, we had to use two stages: One at the top of the vacuum chamber and two at the end of each arm.

Figure 4.2.: Experimental setup

The radial density distribution of metastable argon is quantified by laser absorption spectroscopy. The schematic of the experiment is depicted in fig. 4.2. At the top of CH1 an U-shaped frame made of Item alloy profiles is mounted on a translation stage with which it can be shifted in y- and z-direction. The exact position can be aligned with a millimeter screw. On one arm of the frame a laser beam is coupled out of a fiber and collimated and on the opposite side a silicon laser diode is mounted. A tunable diode laser (DL pro from Toptica Photonics) which is adjusted to the cooling transition (λ = 811.754 nm is used as light source. As power broadening of the spectroscopy should be avoided, the laser beam's intensity is comparably low ($I \approx 0.5\,\mu W\,mm^{-2}$). Since the whole setup is stable against vibrations it allows reproducible measurements. The

[1] Slower atoms enhances the effectiveness of the collimator.

wavelength of the laser was modulated with a sawtooth voltage. This allows to scan the whole Doppler profile of the transition which provides additional information on the plasma such as temperature and speed of the atoms. To suppress disturbing ambient light a spectral bandpass filter is installed in front of the detector. An oscilloscope reads out the detector signal.

Since the three-dimensional distribution of metastable atoms is of interest, the plasma cloud is scanned through in slices that are parallel to the xy-plane. The step width is 1 mm and the stage's maximum traveling distance is 30 mm which results in 30 data points.

Additionally, it is necessary to measure a background signal at each position because the glass window's transmissivity has a strong frequency dependence that is furthermore highly spatial dependent. Consequently, the plasma source was turned off after each measurement and a background signal was recorded. This requires a good impedance matching between the antenna and the amplifier, so that the plasma remains the same after switching on and off.

Apart from that, a Doppler free saturation spectroscopy and a Fabry-Pérot interferometer signal is recorded which is used for the frequency calibration of the absorption spectroscopy profiles.

4.2. Measurements

4.2.1. Abel transform

The absorption signal observed at a position y_k is equal to the optical depth [11]

$$od_0(y_k, z) \equiv \sigma_0 \int n(x, y_k, z)\mathrm{d}x \simeq -\ln\left(\frac{I_t}{I_i}\right), \tag{4.1}$$

where σ_0 is the cross section of the transition, I_t the intensity transmitted through the plasma and I_i is the incident intensity. This is the integral over the atomic density $n(x, y_k, z)$ along the light path (in x-direction), which comes directly from Lambert-Beer law

$$\frac{\mathrm{d}I}{\mathrm{d}x} = -n\sigma_0 I. \tag{4.2}$$

This section is mainly oriented at [12].

The challenge is to reconstruct the two-dimensional distribution of the atomic density from the measured projection in y-direction. This is similar to the procedure in computer tomography.

In the given situation we can assume radial symmetry around the center of the plasma tube which allows us to use the so called *Abel transformation* (fig. 4.3) that describes the relation between the radial distribution $f(r)$ and its measured projection

$$h(y) = 2\int_y^\infty f(r)\frac{r}{\sqrt{r^2-y^2}}\mathrm{d}r. \tag{4.3}$$

The reconstruction of the unknown function $f(r)$ from the measured data $h(y)$ can be executed analytically with the inverse Abel transform

$$f(y) = -\frac{1}{\pi}\int_y^\infty \frac{\mathrm{d}h(y)}{\mathrm{d}y}\cdot\frac{\mathrm{d}y}{\sqrt{y^2-r^2}}. \tag{4.4}$$

In practice however, $h(y)$ isn't given as an analytical function but as a set of N discrete data points. Many algorithms were developed to calculate $f(r)$ numerically. In this work, the matrix method and the Fourier method were examined.

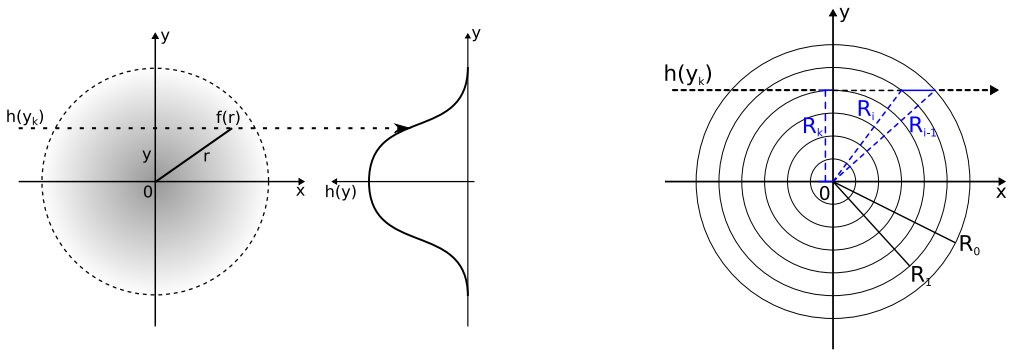

(a) Basic Principle of Abel transform. $h(y_k)$ can be understood as an integration over the atomic density along the light path in x-direction at a certain height y_k. We are interested in the radial density distribution $f(r)$.

(b) Matrix method of Abel transform. We assume that the real function $f(r)$ can be be approximated by N rings. Indexes are counted from outside to the center. This also applies for the measured projection h_k).

Figure 4.3.: Abel transform. The left picture illustrates the basic principle and the right one shows explaines the matrix mathod.

Matrix method We assume that the real radial distribution $f(r)$ can be approximated by N discrete concentric rings with

$$f(r) = f_k = \text{const.}, \quad \forall R_{k-1} > r \geq R_k \quad (k = 1, \ldots, N). \tag{4.5}$$

With the considerations in fig. 4.3b one obtains the relation

$$h_k = \sum_{i=1}^{k} \underbrace{2 \cdot \left(\sqrt{R_{i-1}^2 - R_k^2} - \sqrt{R_i^2 - R_k^2} \right)}_{\equiv a_{ik}} f_i, \tag{4.6}$$

where h_k are the measured profile points.

The matrix A which consists of the matrix elements a_{ik} is triangular and hence can be inverted which yields f_i.

This method was implemented in a Matlab® function during this work.

Fourier method A new approach was proposed in [13] that is based on a cosine expansion of the radial distribution

$$f(r) = \sum_{n=N_l}^{N_u} A_n f_n(r), \tag{4.7}$$

with the unknown amplitudes A_n where N_u and N_l defines the upper and lower limit of the expansion and

$$f_0(r) = 1; \quad f_n(r) = 1 - (-1)^n \cos\left(n\pi \frac{r}{R}\right). \tag{4.8}$$

From eq. (4.3) follows that

$$H(y) = 2 \sum_{n=N_l}^{N_u} A_n \int_y^\infty f_n(r) \frac{r}{\sqrt{r^2 - y^2}} \mathrm{d}r. \tag{4.9}$$

The integrals

$$h_n = \int_y^\infty f_n(r) \frac{r}{\sqrt{r^2 - y^2}} \mathrm{d}r \tag{4.10}$$

must be calculated numerically in advance. In order to obtain the amplitudes A_n we use the fact that the function $H(y)$ represents the measured data $h(y_k)$ with $1 \leq k \leq N$. We write this as a least-squares criterion

$$\sum_{k=1}^{N} [H(y_k) - h(y_k)]^2 \stackrel{!}{=} \mathrm{Min}\,. \tag{4.11}$$

Inserting eq. (4.9) and differentiation with respect to A_n yields an equation system

$$2\sum_{n=N_l}^{N_u}\left(A_n\sum_{k=1}^{N}h_n(y_k)h_m(y_k)\right)=\sum_{k=1}^{N}h(y_k)h_m(y_k),\quad \forall m\colon\ N_l\le m\le N_u\,, \tag{4.12}$$

that can be solved on a computer. Hence we obtain values for A_n and the resulting radial distribution $f(r)$. A matlab code for this algorithm is provided in [14].

4.2.2. Results and interpretation

One major problem is the small traveling distance in y-direction. A translation stage with 15 mm was used. This wasn't enough so an additional translation stage was mounted at each arm of the U-profile which gave us another 15 mm. At first, the height of the laser beam was only shifted by moving the translation stage. When it reached its end, the two stages at the arms where moved upwards and the upper stage downwards again for the same amount. Then the next 15 mm were measured by moving the upper stage. This was enough to measure one slice of 30 mm close to the tube. The great disadvantage of this setup is that misalignments can occur while moving the small stages at the end of the arms.

Two types of profiles were recorded: One that starts about 15 mm below the center of the plasma tube and monitors the complete cross section. This gives information on the symmetry of the plasma cloud and its center. The other started in the middle of the tube and went 30 mm upwards. Only this one can be used for the Abel inversion since a reliable Abel transformation only functions if the intensity goes to zero in the outer region.

We could observe three different plasma modes. The first one occurs at low pressures ($< 3.5\times10^{-5}$ mbar). The plasma is confined to the plasma tube and rises only some centimeters out of the tube. It has the shape of a candle flame. The second occurs at mid pressures (3.5×10^{-5} mbar to 4.5×10^{-5} mbar). The plasma fills out the whole vacuum chamber. The third mode appears at even higher pressures. It is similar to the second one, but gleams stronger. As the plasma and the metastable density doesn't decline to zero here, mode two and three aren't suitable for the Abel transform.

Figure 4.4a on the next page shows a scan through the center of the plasma at a distance of about 1 cm from the plasma tube. As the intensity of the laser beam is with $I_l \approx 0.5\,\mathrm{W\,m^{-2}}$ small compared to the saturation intensity of the cooling transition $I_s = 28.8\,\mathrm{W\,m^{-2}}$ saturation effects can be neglected. A surprising feature of the profile is the fact that two peaks close to the center are visible instead of one which as in the

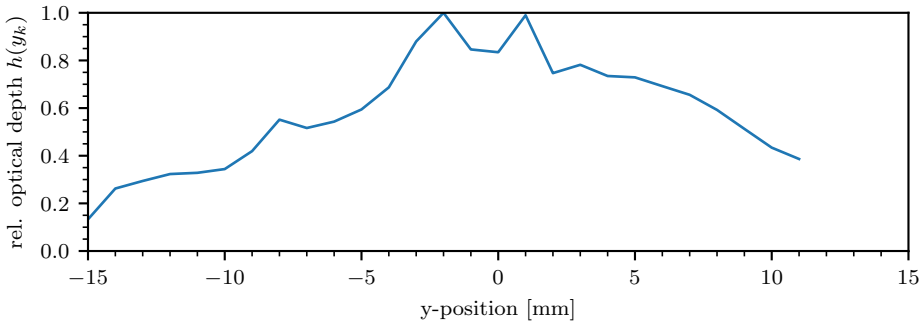

(a) Scan through the plasma cloud from 15 mm below the plasma tube's center to 15 mm above. The shows the measured optical depth relative to the maximum. It is surprising that the profile has two peaks close to the center instead of one which indicates that the radial distribution of metastables isn't Gaussian.

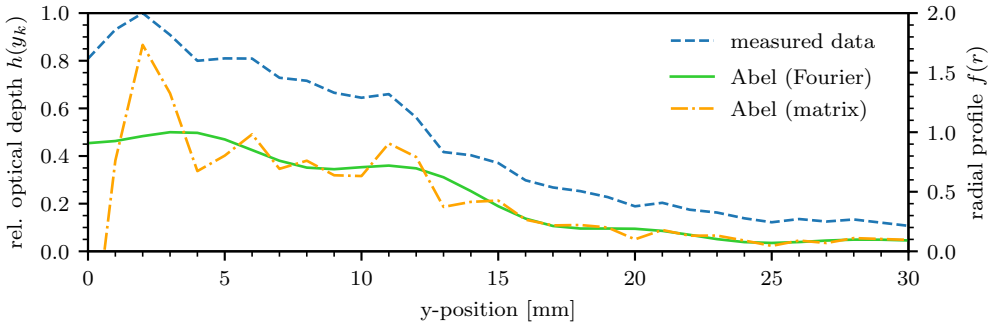

(b) Scan from the plasma tube's center to 30 mm above. This profile shows similar features as that in fig. 4.4a. It hat also a maximum some millimeters next to the center and a step at about 10 mm. The profile was Abel inverted to obtain the radial distribution. Both methods, the matrix and the Fourier method, were applied. They lead to similar results which support a non-Gaussian distribution.

Figure 4.4.: Measuring results of the experiments at the OpTTA apparatus. The profiles were redorded at a distance of approximately 10 mm away from the end of the plasma tube. The laser beam intensity was about $0.5\,\mathrm{W\,m^{-2}}$, which far below the saturation intensity of the cooling transition and the pressure was in the order of 3×10^{-5} mbar. Note that we measured the distribution of metastable argon atoms rather than the plasma distribution.

Gaussian radial distribution. This is a strong indicator that the radial distribution of metastable argon atoms has the shape of a ring where the densest area is not at the center but some millimeters away. The question in this case is how reliable the data is. This structure might originate from statistical noise, fluctuations in the plasma intensity which might occur because we have to reignite the plasma after each measuring point or dirt on the glass window of the vacuum chamber. This feature however is present in more or less all of our measured profiles in a qualitative similar way so we can conclude that a non-Gaussian distribution is realistic.

A scan from the center of the tube to the top is depicted in fig. 4.4b on page 28. Additionally, an Abel inversion was carried out with both methods. The Abel inversion is very critical to the correct choice of the zero-point. Here, figure (a) can help. Generally, both the matrix and the Fourier method are suitable for the Abel transform. They show mainly the same radial distribution. The great advantage of the Fourier method is that finite cosine expansion behaves like a build-in low-pass filter that suppresses automatically noise in the measured $h(y_k)$ profile. The behavior and strength of this filter can be adjusted by choosing a lower expansion limit for a stronger suppression of noise which might eliminate features however. We achieved good results with an expansion up to an order of $N = 10$. The matrix method is more sensitive to noise because it has no filter. Therefore, the data should be preprocessed and the $h(y_k)$ should be smoothed before the transformation, which we didn't do here.

The results of the Abel inversion support the presumption that the three-dimensional shape of the metastable argon density is that of a stretched donut[2] rather than an ellipsoid. This conclusion is consistent which the result of [15] where the authors performed a similar experiment. They also measured the radial distribution of metastable argon in a RF plasma discharge and found out that densest region are close to the walls instead of in the center. The charged particles in the plasma shield the RF field and hence reduce the field strength in the interior of the plasma.

In addition more information can be exploited from the measured absorption profiles. The variance σ of the Gaussian gives information about the temperature of the gas according to eq. (2.9) on page 6. We get a temperature of $\approx 300\,\mathrm{K}$, which lies a bit below the temperature of the closed plasma cell. Yet, σ or the temperature isn't suitable for an Abel inversion so a determination of a radial temperature profile isn't possible. The variance σ is plotted in fig. 4.5 on the following page. It strikes that *sigma* increases for higher y-positions. This is probably due to the fact that only the faster atoms are able to reach the higher y-positions.

[2]The correct scientific term would be torus.

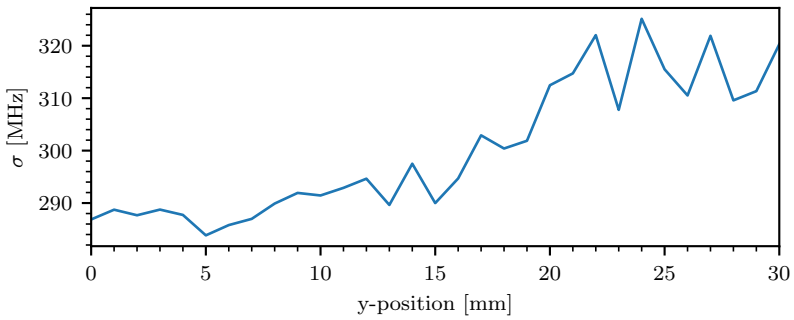

Figure 4.5.: Variance σ of the measured Doppler profile as a function of the y-position. The variance can provide information about the temperature of the metastable atoms. This strikes that the variance increases for large y-positions. The reason is probably that only the hotter atoms are able to reach a reagions far away from the plasma tube.

The experimental setup can be improved by using a translation stage with a larger traveling range. There are models with automatic piezo available. With such a device a fully automated measuring procedure could be realized that enables us to measure many scan slices at different z-positions in a reasonable amount of time which would provide a whole three-dimension image of the density distribution. For determining the precise center of the plasma tube, a laser beam can be aligned in z-direction. This was also planned in the scope of this work. Unfortunately, the experiment had to pause due to technical reasons and prevented further investigations.

5. Summary and outlook

Fortunately, the five fiber-coupled closed spectroscopy cells were finished by the workshop just in time so that we were able to assemble one and test it. The results of the saturated absorption spectroscopy look good and soon all five modules will be available for their application in the routine ArTTA-10ml apparatus.

The five helical resonators work well in combination with the closed plasma cells. The plasma have burned continuously stable for some weeks now. It showed that the ignition point for the plasma is reproducible and requires little RF-power.

The filling process of the argon plasma cells proved to be a reliable method for manufacturing the plasma cells. We experienced that one cell last about half a year which is enough for an application in the fiber-coupled closed spectroscopy cells. As mention in section 3.2 on page 12, it is planned to improve the filling apparatus by installing a gauge for monitoring the pressure and a spectroscopy to examine the involved substances.

Three-dimensional measurements of the density distribution of metastable argon atoms in the source chamber of the OpTTA apparatus brought interesting results. From the graphs we can conclude that the radial distribution isn't Gaussian but has its maximum some millimeters away from the center. The general concept with the experimental setup and the Abel transform proved to deliver useful results. However, the setup should be improved, for instance by installing a better translation stage with a larger traveling range and a piezo motor that allows the automation of the measuring procedure. This optimized setup can then be used for a complete three-dimensional mapping of the metastable distribution.

Sound knowledge about this can lead to a redesign of the source chamber. For instance the collimator can be adapted in order to reduce the loss of metastables by collisions with the walls. Another approach is to replace the existing RF-antenna by a helical resonator. This can have the advantage of a lower RF-power needed for the ignition of the plasma as long as the performance of metastable production is not lower. Furthermore the impedance matching of the antenna would drop out because the helical resonator has a well defined grounding.

A. Appendix

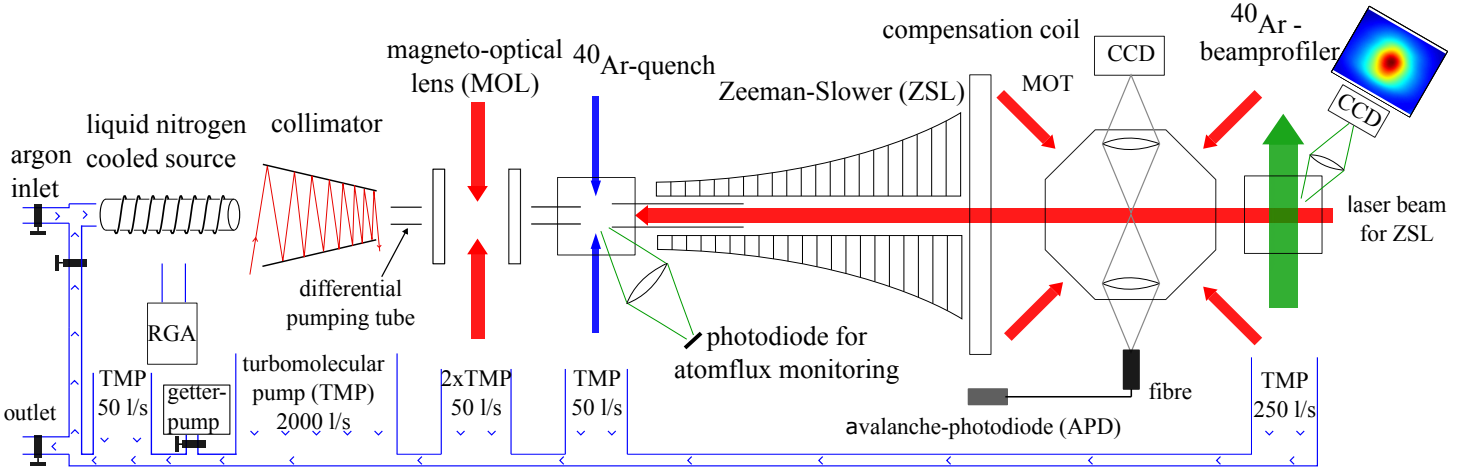

Figure A.1.: Schematic of the current ArTTA apparatus that is used for water dating with ^{39}Ar . For detailed information plese refer to [1], which is the origin of this schematic.

Acknowledgements

At this point I would like to say thank you to all that have contributed to this work:

- many thanks to Markus K. Oberthaler who gave me the opportunity to write this Bachelor Thesis and supported me with clever ideas and expert knowledge.
- Selim Jochim, who consent to do the second correction for my bachelor thesis.
- Lisa Ringena und Zhongyi Feng for their great support of my work. You always had a sympathetic ear and I could learn a lot about the lab business. Also thanks for your time and effort in proofreading.
- my office colleagues Celia Viermann, Maurus Hans and Helmut Strobel for the relaxed atmosphere and the nice conversations on the side.
- my ATTA colleagues Sven Ebser and Maximilian Schmidt for your advice on all questions concerning physics and beyond.
- Alex Impertro for a relaxed FP-time and for proofreading this paper.
- to the entire Matterwave workgroup for the great time.
- my special thanks go to Hannes Riechert for his magnificent help on recovering the data of my thesis from my damaged hard disk drive, when the super MCA of any bachelor happened to me.
- and last but not least to my parents Elke and Hans Gierlich and my sister Martina who always supported me.

Bibliography

[1] Florian Ritterbusch. "Dating of groundwater with Atom Trap Trace Analysis of ^{39}Ar". PhD thesis. Faculty of Physics and Astronomy, University of Heidelberg, 2013.

[2] Joachim Welte. "Atom Trap Trace Analysis of ^{39}Ar". PhD thesis. Faculty of Physics and Astronomy, University of Heidelberg, 2011.

[3] Wolfgang Demtröder. *Laserspektroskopie*. 2007.

[4] Peter van der Straten H. J. Metcalf. "Laser Cooling and Trapping of Neutral Atoms". In: *The Optics Encyclopedia*. 2007.

[5] "Saturated Absorption Spectroscopy". Instruction of a Advanced Physics Laboratory course. University of Florida – Department of Physics.

[6] Michael A. Lieberman and Allan J. Lichtenberg. *Principles of Plasma Discharges and Material Processing*. 2005.

[7] W. W. Macalpine and R. O. Schildknecht. "Coaxial Resonators with Helical Inner Conductor". In: *Proceedings of the IRE* (1959).

[8] Zhongyi Feng. "Implementierung einer Atomflussüberwachung für ^{39}Ar ATTA". Bachelor thesis. Faculty of Physics and Astronomy, University of Heidelberg, 2012.

[9] Felix Hahne. "Stabilisierung und Implementierung einer Echtzeit-Flussbestimmung von metastabilem Argon". Bachelor thesis. Faculty of Physics and Astronomy, University of Heidelberg, 2017.

[10] Florian Ritterbusch. "Realization of a collimated beam of metastable atoms for ATTA of Argon 39". Diploma Thesis. Faculty of Physics and Astronomy, University of Heidelberg, 2009.

[11] G. Reinaudi et al. "Strong saturation absorption imaging of dense clouds of ultracold atoms". In: *Optics Letters* (2007).

[12] G. Pretzler. "Comparison of Different Methods of Abel Inversion Using Computer Simulated and Experimental Side-On Data". In: *Zeitschrift für Naturforschung a* (April 1992).

[13] G. Pretzler. "A New Method for Numerical Abel-Inversion". In: *Zeitschrift für Naturforschung* (1991).

[14] *Abel Inversion Algorithm - File Exchange - MATLAB Central*. July 26, 2017. URL: https://de.mathworks.com/matlabcentral/fileexchange/43639-abel-inversion-algorithm?.

[15] Masahiro Tadokoro et al. "Two-dimensional density ditribution of metasatble atoms in an inductively coupled plasma in Ar". In: *Physical Rewiew E* (1998).

Don't panic!

Erklärung

Ich versichere, dass ich diese Arbeit selbstständig verfasst und keine anderen als die angegebenen Quellen und Hilfsmittel benutzt habe.

Heidelberg, den 31. Juli 2017,